The pulse-degradation characteristic of ZnO varistors

C. G. Shirley and W. M. Paulson
Motorola, Incorporated, Semiconductor Research and Development Laboratories, 5005 East McDowell Road, Phoenix, Arizona 85008

(Received 2 March 1979; accepted for publication 26 April 1979)

We find that two factors bear on the high-energy pulse degradation of a varistor's electronic characteristic. First, the electronic structure of active grain-boundary segments depends solely on the peak temperature occurring there during a pulse, and second, this peak temperature is determined by the thermal transport properties of the microstructure. We find that the intrinsic electronic structure can be modified without changing the microstructure to greatly improve the pulse-degradation performance of a varistor by an anneal at low temperature (600 °C) in oxygen. The influence of microstructure is embodied in the grain-boundary temperature-magnification factor Z_{gb} which is defined, measured, and studied theoretically. Theory shows that there are three regimes: (i) a long-pulse-width regime where $Z_{gb} = 1$, (ii) a short-pulse-width regime where $Z_{gb} \sim (\text{pulse width})^{-1/2}$, independent of pulse energy, and (iii) a very-short-pulse-width (or high-energy-density) regime where $Z_{gb} \sim (\text{pulse energy})^{-1/2}$, independent of the pulse width. The theory contains one microstructural parameter. Our data encompasses the first two regimes and agrees well with theory for a value of the microstructural parameter which is in good agreement with earlier work.

PACS numbers: 72.20. – i, 85.20.Ea

I. INTRODUCTION

The ZnO varistor (or metal-oxide varistor, MOV) is a complicated multiphase ceramic which has a highly nonlinear current-voltage characteristic similar to back-to-back Zener diodes. In contrast to the Zener diode, however, the MOV has a much greater current and voltage handling capability than an equivalently priced Zener diode. This has made the MOV particularly attractive for transient suppression applications. Although there has been considerable experimental[1–4] and theoretical[5–8] effort devoted to elucidate the electronic properties of the intergranular phase (or doped grain boundary) which gives the MOV its unique properties, little has been done to study the mechanism of degradation when the MOV is subjected to energetic electrical pulses. This, combined with the practical significance, prompted the present study.

In the transient suppression application the varistor is placed in shunt across the power supply to the component to be protected. Under normal conditions the ac or dc bias does not exceed the turn-on voltage, but a high-voltage transient appearing on the line will turn the MOV on and will be shorted to ground. In extreme cases of overload, the damage will consist of a pinhole punch-through or other visible catastrophic failure. In less extreme cases, there is no visible damage but a change in electrical characteristics occurs. One aspect of this change is that the current-voltage characteristic becomes asymmetric and often the breakdown voltage in one or both directions is lowered. If the reduction in the turn-on voltage exceeds about 10% of the unpulsed nominal turn-on voltage, the increased leakage which occurs when the normal operating bias is restored will be sufficient to further degrade and eventually cause thermal runaway in the varistor. From a practical point of view, it is the noncatastrophic shift in the current-voltage characteristic immediately after a pulse which determines the pulse-degradation limitations of the varistor.

Our experiments suggest that these shifts are caused by reversible changes in the electronic properties of the intergranular phase. The detailed nature of these changes is an interesting object of study, but it is not the focus of the present paper. This is because the relationship between the pulse parameters (pulse voltage, pulse current, pulse energy, and pulse width) and degradation, i.e., the pulse-degradation characteristic, depends on the thermal transport properties of the varistor microstructure as well as the electronic properties of the active intergranular phase, and it is the thermal transport properties which account for most of the functional dependence of the pulse-degradation characteristic on pulse parameters. A model in which the shift in electronic properties is a function solely of the maximum temperature seen by the intergranular phase and which uses thermal transport properties to relate this temperature rise to the pulse parameters gives an adequate description of our data.

II. EXPERIMENTAL

Although there are four pulse parameters, only two are independent since the pulse current density J_p and the pulse electric field F_p are related through the current-voltage characteristic, and the pulse energy density is given by

$$\mathscr{E}_p = J_p F_p t_p, \tag{1}$$

where t_p is the pulse width. Experimentally, the convenient independent parameters were the pulse current and pulse width, and we studied degradation as a function of these. The varistors used in this study were made in our laboratory by wet mixing oxide powders with a little water-soluble organic binder in the following proportions: 1.0% Bi_2O_3, 0.5% Co_2O_3, 1.0% MnO_2, and 0.5% Sb_2O_3 with the bal-

 0021-8979/79/095782-08$01.10

ance ZnO (mole percentages). The granulated mixture was pressed into disks and fired in air at 1300 °C for 1 h. Radial leads were attached by solder dipping after evaporative metallization (Ti/Ni/Ag) of both disk faces. Pulses were generated by a Velonix 660 pulse generator for pulses down to 100 μsec and by an SCR-crowbarred SCR discharge of a capacitor for shorter pulse widths (down to 5 μsec). The pulse current and voltage were observed on a dual-trace storage oscilloscope. The Velonix pulses were rectangular, whereas the SCR-crowbarred pulses had an exponential rise and decay.

Since the lot contained only 16 varistors, we carried out some preliminary experiments to see if the electrical degradation could be annealed out at 600 °C in flowing oxygen so that the varistors could be reused in the experiment. This was done by taking a single varistor through a careful sequence of measurements of the current-voltage characteristic and annealing treatments. An (unannealed) varistor was taken directly from our process, and its I-V characteristic was measured. The current was kept below 1 mA to eliminate heating effects. The varistor was then subjected to a 265-V 20-A 2-msec (10.6-J) pulse and its I-V was measured immediately (within 10 sec of the pulse) and 21 h after the pulse in both the forward and reverse directions. The forward characteristic has the measuring current flowing in the same direction as the pulse current. The characteristics are shown in Fig. 1. The unpulsed characteristic was symmetrical, but the two pulsed characteristics show a considerable increase in the leakage current, especially in the reverse direction. However, the reverse leakage is seen to recover slowly, tending to make the varistor more symmetrical. The change in the characteristic immediately after a pulse is both a convenient and a practically significant measure of degradation. The leads and metallization were removed from the varistor of Fig. 1 and it was annealed on an alumina substrate under flowing oxygen at 600 °C for 1.5 h after which leads were reattached. The I-V characteristics were taken both before and immediately after pulsing with a 261-V 20-A 2-msec pulse. These two characteristics are shown in Fig. 2. The unpulsed characteristic of the annealed varistor was symmetrical and showed considerably smaller leakage than the unpulsed characteristic in Fig. 1. Moreover, the pulsed annealed characteristic (Fig. 2) was more symmetrical and showed less degradation than the corresponding pulsed unannealed characteristic (Fig. 1). Note that both unannealed and annealed parts were subjected to almost identical pulses. The leads were again removed from the varistor and the annealing, lead attach, measurement, pulse, and remeasure sequence was repeated with results almost identical to those of

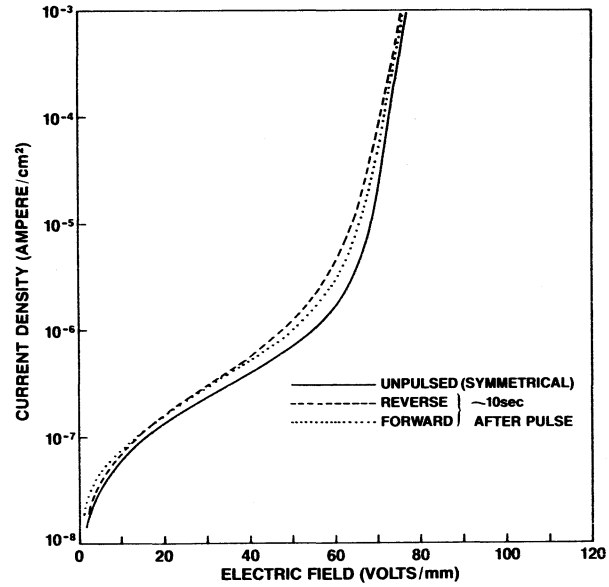

FIG. 2. Current-voltage characteristic of the varistor of Fig. 1 after annealing at 600 °C for 1.5 h in flowing O_2 (solid curve), and after another 261-V 20-A 2-msec pulse.

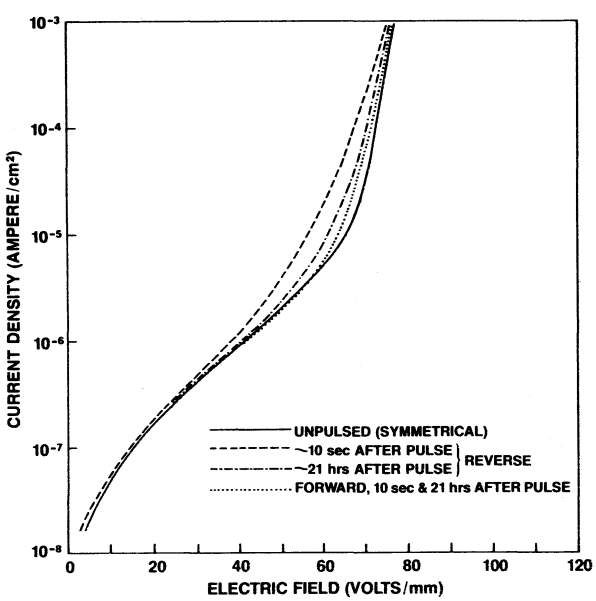

FIG. 1. Current-voltage characteristics of an unannealed Motorola experimental varistor (263CC3) before and after a 265-V 20-A 2-msec (10.6-J) pulse.

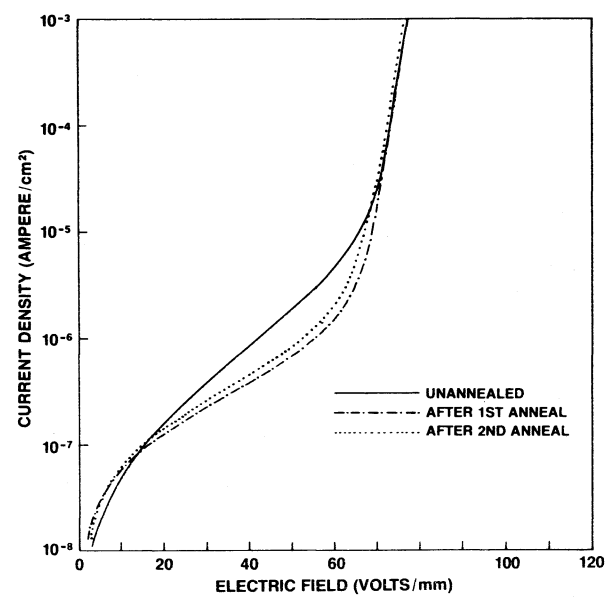

FIG. 3. Comparison of the unannealed unpulsed current-voltage characteristic with the current-voltage characteristic of the same varistor after successive anneals. The varistor is the same as that in Figs. 1 and 2, and two of the curves are taken from Figs. 1 and 2. All characteristics are symmetrical.

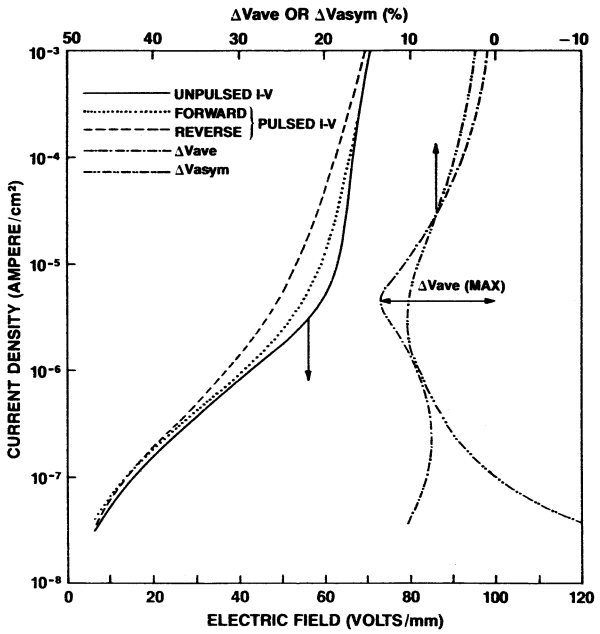

FIG. 4. Current-voltage characteristic of unannealed varistor before and after a 2-msec 20-A 250-V (81-J/cm ^{3}) pulse. ΔV_{ave} and ΔV_{asym} defined in Eqs. (2) are also plotted. The peak value in ΔV_{ave} (indicated) is used as a measure of the pulse degradation.

Fig. 2. In Fig. 3 we compare the unpulsed characteristic obtained after this second anneal with the unpulsed characteristics immediately after the first anneal and directly out of our process with no anneal (from Figs. 2 and 1, respectively). It is clear that the annealing step serves two functions: changes in the electronic nature of the active intergranular phase which results in lower leakage and improved pulse-degradation performance.

(2) Annealing can be used to erase the pulse history of a previously annealed varistor to reasonable accuracy as evidenced by Fig. 3. Actually, there is a tendency for leakage to increase with repeated anneals, but the changes between anneals had no discernible correlation with the pulse-degradation properties of the varistor. That is, to within experimental scatter, a given pulse gave the same degradation irrespective of the particular varistor or anneal, for the annealed varistors.

To study degradation as a function of pulse parameters it is necessary to find a convenient and simple way to characterize the degradation of a varistor by a single preferably dimensionless number. We programmed our data-acquisition system to plot the percent average deviation and asymmetry of the I-V characteristics in addition to the characteristics themselves, as shown in Fig. 4. These dimensionless parameters are defined as follows:

$$\Delta V_{ave} = 100\{1 - [V_a(+) + V_a(-)]/2V_b\}, \quad (2a)$$

$$\Delta V_{asym} = 100[V_a(+) - V_a(-)]/V_b, \quad (2b)$$

where $V_a(+)$ and $V_a(-)$ are the forward and reverse characteristics, respectively, after the pulse, and V_b is the characteristic before the pulse. For our varistors we noted that the percent average deviation usually had a distinct peak near the knee in the I-V characteristic, and we used its value, denoted by ΔV_{ave} (max), as our measure of degradation. This choice has the advantage of being independent of measurement errors in both electrode area and disk thickness.

These preliminary observations lead us to the experimental plan illustrated in Fig. 5. Unannealed varistors were taken directly from our process and subjected to single rectangular pulses with pulse widths varying from 250 μsec to 2 msec and pulse currents varying from 20 to 5 A. Each varistor could be subjected to only one pulse in the unannealed state since the undamaged unannealed state could not be restored after pulsing. The leads were then removed and the varistors were annealed in the same way as in the preliminary experiments, and the varistors were again subjected to a matrix of pulses. In contrast to the unannealed varistors, however, memory of the pulses could be erased by a subsequent annealing step so a relatively large amount of data for the annealed state could be acquired by cycling the lot through several such steps, three altogether. For the annealed varistors we used pulses as short as 5 μsec.

It is easy to show that practically all of the energy dissipation in a varistor occurs in the electrically active grain-boundary phase which determines the I-V characteristic. For a short pulse of a given energy it is physically reasonable to expect that the peak grain-boundary temperature rise will exceed that of the grain centers since the heat cannot be conducted rapidly enough away from the grain boundaries to maintain a uniform temperature distribution during the pulse. On the other hand, for a long pulse of the same total energy, the temperature rise will be the same everywhere, including grain boundaries, since the heat will have ample time to diffuse into the grains. We shall confirm in a moment that pulse widths longer than 2 msec fall into the long-pulse width (uniform-temperature-rise) regime. We must emphasize that the pulses and pulse widths we are discussing are all short enough that the heat has no time to diffuse from the ceramic body down the leads or to be removed by convection *during the pulse*. A thermal response analysis shows that the cooling-time constant for these processes is in the neighborhood of 1 or 2 sec. Our pulse tester could not supply pulses

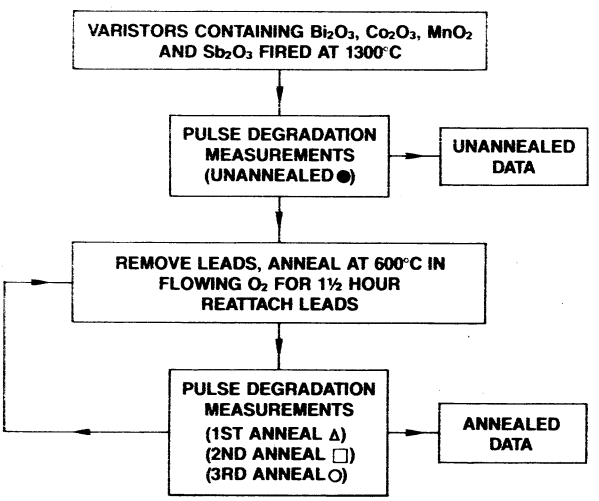

FIG. 5. Experimental plan for obtaining data for unannealed and annealed varistors. Annealing was also used to erase the memory of earlier pulses so more data could be obtained. Plot symbols for data in Figs. 6–8 are defined.

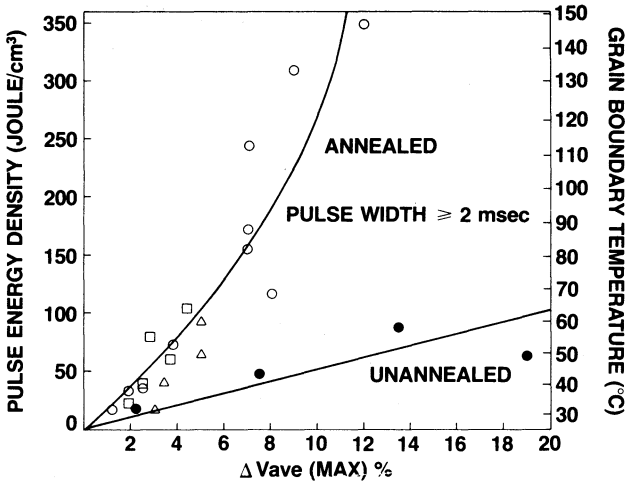

FIG. 6. Pulse energy density or peak grain-boundary temperature [via Eq. (3)] versus pulse degradation [see Fig. (4)] for annealed and unannealed varistors in the long-pulse-width regime.

longer than 2 msec, but it could supply up to eight repeated 2-msec pulses within 150 msec, so from the standpoint of the peak (uniform) temperature rise, we had pulses to 16 msec available. In Fig. 6 we plot the energy density as a function of $\Delta V_{\rm ave}$(max) for pulse widths greater than 2 msec for both the annealed and the unannealed varistors. Since all points in this plot are in the long-pulse-width regime where the temperature rise is spatially uniform, we may write the peak grain-boundary temperature rise as

$$\Delta T_{gb} = \mathscr{E}_p/\rho C \quad \text{(long pulse widths)}, \tag{3}$$

where ρ is the ceramic-body density and C is its specific heat. Equation (3) may be used to recalibrate the curves in Fig. 6 in terms of the peak grain-boundary temperature. See the right-hand scale. The considerable improvement of the pulse-degradation performance obtained by annealing is striking in Fig. 6. Parabolic and linear best fits, forced through the origin, to the annealed and unannealed data, respectively, are also shown in Fig. 6. The curve for the annealed data tends to indicate that degradation is solely a function of the maximum $T_{\rm gb}$ reached during a pulse since all the data falls reasonably well on a common curve in spite of variations in pulse current and pulse width which gave roughly the *same* energy in several cases. That is, the degradation seems to depend much more weakly on J_p than on the peak value of $T_{\rm gb}$.

If we assume that the measure of degradation depends solely on the peak grain-boundary temperature reached during a short pulse, as well as for the long pulses, then the empirical relationships in Fig. 6 may be used as grain-boundary temperature "thermometers" for the short pulses (<2 msec). For short pulses, the peak temperature rise at a grain boundary during (i.e., just at the end of) a pulse, $\Delta T_{\rm gb}$, will exceed the average temperature rise based on the total energy density of the pulse, $\Delta T_{\rm ave}$ ($\equiv \mathscr{E}_p/\rho C$), because of the finite time needed for the heat to traverse a grain. Note that $\Delta T_{\rm ave}$ is the uniform temperature rise of the ceramic body long after the pulse but before heat has escaped through the package. We define the grain-boundary temperature-magnification factor $Z_{\rm gb}$ as

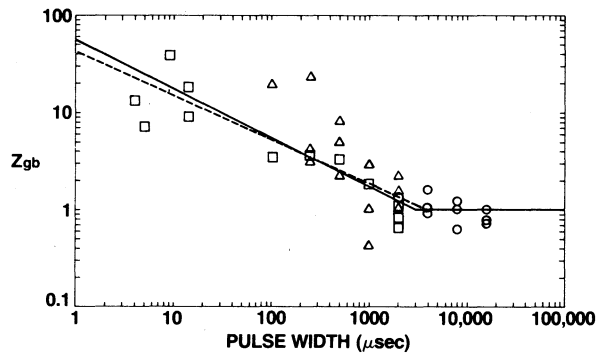

FIG. 7. Grain-boundary temperature-magnification factor as a function of pulse width for annealed varistors. The unconstrained best fit (broken line) has slope -0.453. The best fit constrained to have slope $-\frac{1}{2}$ is the solid sloping line.

$$Z_{\rm gb} \equiv \Delta T_{\rm gb}/\Delta T_{\rm ave} = \rho C \Delta T_{\rm gb}/\mathscr{E}_p. \tag{4}$$

The factor $Z_{\rm gb}$ must satisfy $Z_{\rm gb} \geqslant 1$, with $Z_{\rm gb} = 1$ in the long-pulse-width uniform-heating regime. Equation (4) may be used in conjunction with the curves in Fig. 6 to measure $Z_{\rm gb}$ as a function of pulse width. For a given pulse $\mathscr{E}_p$ is determined from the pulse parameters and the ceramic body dimensions, while $\Delta V_{\rm ave}$(max) is deduced from I-V characteristics taken before and immediately after the pulse. The value of $\Delta T_{\rm gb}$ corresponding to this value of $\Delta V_{\rm ave}$(max) can be read off Fig. 6 and substituted with $\mathscr{E}_p$ into Eq. (4) to determine $Z_{\rm gb}$. This has been done for both the annealed and unannealed varistors and the results are given in Figs. 7 and 8.

In Sec. III theoretical consideration of the thermal properties of the varistor microstructure shows that a logarithmic plot of $Z_{\rm gb}$ against pulse width has three portions: (i) a long-pulse-width regime where $Z_{\rm gb} = 1$, (ii) a short-pulse-width regime where $Z_{\rm gb} \sim t_p^{-1/2}$ and is independent of pulse energy, and (iii) a very-short-pulse-width regime where $Z_{\rm gb}$ depends only on pulse energy and is independent of pulse width. Only the first two regimes are represented in our data. To determine the slope and extent of the short-pulse-width portion of the logarithmic $Z_{\rm gb}$–vs–pulse-width plot in Fig. 7 successively more data points, starting with short pulse widths, were used to fit a straight line through the (logarithms of) the data points. It is clear that for "perfect" data the slope of this line will be constant until points on the

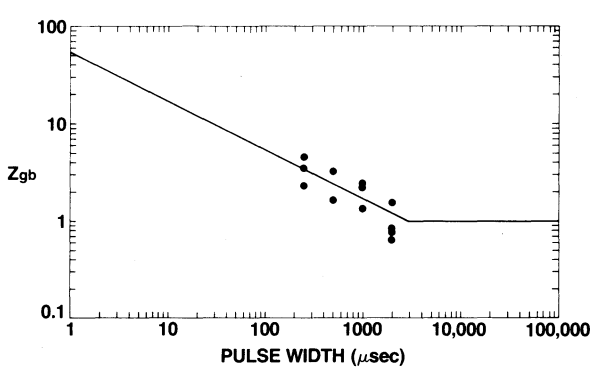

FIG. 8. Grain-boundary temperature-magnification factor as a function of pulse width for unannealed varistors. The $-\frac{1}{2}$ slope best fit is shown.

$Z_{gb} = 1$ (long-pulse-width) portion are included, at which juncture the magnitude of the slope will begin to decrease. Thus we stopped adding points to determine the sloping portion of the plot just before the magnitude of the slope began to decrease. The line determined in this way is shown as a dashed line with slope -0.453 in Fig. 7. This value is good confirmation of the theory. The value of the pulse width at the break in the Z_{gb}-vs-t_p plot is an interesting quantity to analyze in terms of the model below. The best value of this pulse width for the model is obtained by assuming the correctness of the model, i.e., a slope of $-\frac{1}{2}$, and making a least-squares fit constrained to have a slope of $-\frac{1}{2}$. The curve so obtained is shown as a solid line in Fig. 7. Note that the determination of which data points lie in the long-pulse-width regime is unambiguous. Since there is too little data for an unconstrained best fit, only a slope-constrained best fit was made to the unannealed data in Fig. 8. Note the agreement between the two Z_{gb}–vs–pulse-width characteristics in Figs. 7 and 8 in spite of the marked differences in the curves in Fig. 6 for the annealed and unannealed varistors. We shall see that the Z_{gb}-vs-t_p characteristic depends just on microstructure, not electronic properties of the intergranular phase. Microstructurally, the annealed and unannealed varistors are identical. Finally, we see that the assumption that the long-pulse-width regime is $t_p > 2$ msec on which the curves in Fig. 6 were based is not quite correct. Actually, the long-pulse-width regime for our varistors is $t_p > 3$ msec, however, considering the scatter in the data the error introduced by this is negligible. The error in this assumption is reflected in the slight displacement in the annealed data points near the origin of Fig. 6 towards higher values of $\Delta V_{ave}(\max)$ than the best-fit curve.

III. THEORY

A model of the pulse-degradation characteristic of the varistor should relate a measure of degradation [say $\Delta V_{ave}(\max)$] to two independent pulse parameters which in this section we shall choose to be the pulse width and pulse energy. The usefulness of our model in describing the pulse degradation depends on the assumption that the degradation is solely a function of the peak grain-boundary temperature occurring during a pulse, i.e.,

$$\Delta V_{ave}(\max) = f[T_{gb}(\max)]. \tag{5}$$

This relationship depends on the detailed properties of the intergranular phase and is to be regarded as an empirical relationship in this paper (Fig. 6) which we shall not attempt to explain theoretically. Our object is to relate $T_{gb}(\max)$ to the independent pulse parameters; specifically the object of study is the grain-boundary temperature-amplification factor Z_{gb}. If the relationship of Eq. (5) does not hold, for example, if $\Delta V_{ave}(\max)$ also depends *directly* on J_p, then the considerations below relating to Z_{gb} are still true but less useful since in this case Z_{gb} will not contain all the functional dependence on pulse parameters.

First, a detailed analytical model for an ideal varistor microstructure will be given, and then modifications to account for a more realistic microstructure will be introduced to interpret our data.

A. Ideal microstructure

If the actual microstructure is idealized as shown in Fig. 9(b), then formally the problem is the one-dimensional idealization shown in Fig. 9(c) since there is no potential drop across the intergranular phase which is parallel to the electric field. Each layer of the intergranular phase is assumed to have a nonlinear current-voltage characteristic such as

$$J = J_0 \left(\frac{v_{gb}}{v_0} \right)^{\alpha}, \tag{6}$$

where J_0 is the current density when the voltage drop across a boundary v_{gb} is equal to the nominal breakdown voltage v_0 and α is the nonlinear exponent ($\alpha = 1$ for Ohmic conduction). Typically, $v_0 = 2$ V for $J_0 = 1$ mA/cm^2 and $\alpha = 40$. The current-voltage characteristic, Eq. (6), is the only property of the intergranular phase which enters into our model. Moreover, the predictions of the model are insensitive to the form of Eq. (6) as long as it is strongly nonlinear. Also, each layer of the ZnO "grain" has the following I-V characteristic:

$$J = \frac{\sigma v_g}{l}, \tag{7}$$

where σ is the electrical conductivity of the ZnO, v_g is the voltage drop across a grain, and l is the grain thickness. Typically, $\sigma = 2\ (\Omega\ \text{cm})^{-1}$ (Ref. 3) and $l = 20\,\mu$. The I-V characteristic of the composite is therefore

$$F = \frac{J}{\sigma} + \frac{v_0}{l}\left(\frac{J}{J_0} \right)^{1/\alpha}, \tag{8}$$

where F is the average electric field between electrodes. Equation (8) shows that the model we are considering takes into account the reversion to Ohmic behavior at high current densities.

The average temperature rise due to a pulse is given by

$$\Delta T_{ave} = \frac{\mathscr{E}_p}{\rho C} = \left(\frac{J_p^2}{\sigma} + \frac{2Q}{l} \right) \frac{t_p}{\rho C}, \tag{9}$$

where Q is given by

$$Q = \frac{1}{2} v_0 J_p \left(\frac{J_p}{J_0} \right)^{1/\alpha}. \tag{10}$$

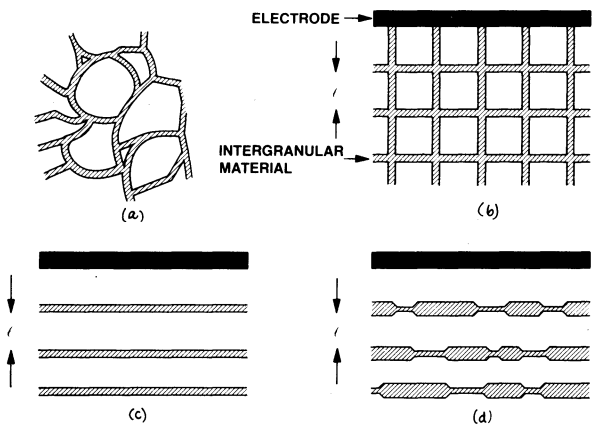

FIG. 9. Idealized models of varistor microstructure; (a) actual structure, (b) idealized structure, (c) simplification of (b), and (d) modification of (c) to account for nonuniform thickness of intergranular phase.

In Eq. (9) $2Ql^{-1}$ is interpreted merely as the portion of the power dissipated in grain boundaries, whereas, below, Q is interpreted as the heat flux from the boundary with the factor $\frac{1}{2}$ in Eq. (10) accounting for equal partition of the flux between grains. For long pulses ΔT_{ave} is also the peak grain-boundary temperature rise. For short pulses, however, account must be taken of the localized nature of the grain-boundary energy dissipation and the consequent spatial- and time-dependent temperature profile across a grain. The temperature profile obeys the following differential equation during a pulse:

$$\rho C \frac{\partial T}{\partial t} = K \frac{\partial^2 T}{\partial x^2} + \frac{J_p^2}{\sigma}, \tag{11}$$

where K is the thermal conductivity of ZnO. The constant terms on the right-hand side of Eq. (11) accounts for Joule heating of the grains. This differential equation must be solved with the following constant-flux boundary conditions:

$$-K \frac{\partial T}{\partial x}\bigg|_{x=0} = K \frac{\partial T}{\partial x}\bigg|_{x=l} = Q.$$

Simple manipulation of the constant-flux boundary-condition solution of the diffusion equation given by Crank[10] gives the grain-boundary temperature rise at the end of a rectangular pulse of duration t_p as

$$\Delta T_{gb} = \left(\frac{J_p^2}{\sigma} + \frac{2QY_{gb}}{l} \right) \frac{t_p}{\rho C}, \tag{12}$$

where

$$Y_{gb} = \frac{1}{y}\left(y + \frac{1}{3} - \frac{2}{\pi^2} \sum_{n=1}^{\infty} n^{-2} \exp(-n^2\pi^2 y) \right), \tag{13}$$

where y is a dimensionless pulse width defined as

$$y = \frac{4\delta t_p}{l^2}, \tag{14}$$

where δ is the thermal diffusivity defined as $\delta = K/\rho C$. For $y \gg 1$, $Y_{gb} \sim 1$, whereas for $y \ll 1$ examination of the asymptotic expansion of the series in Eq. (13) shows that $Y_{gb} \sim 2\pi^{-1/2} y^{-1/2}$. When Eqs. (9) and (12) are substituted into definition (4) we find

$$Z_{gb} = (1-c)Y_{gb} + c, \tag{15}$$

where c, the fraction of the total energy absorbed by the grains, is given by

$$c = \frac{J_p^2 t_p}{\sigma \mathscr{E}_p}. \tag{16a}$$

In Eq. (16) J_p is to be regarded as a function of the independent pulse parameters $\mathscr{E}_p$ and t_p. For the special case of the grain-boundary I-V characteristic of Eq. (6), J_p may be found as a function of $\mathscr{E}_p/t_p$ by solving

$$\frac{J_p^2}{\sigma} + \frac{v_0 J_p}{l}\left(\frac{J_p}{J_0} \right)^{1/\alpha} = \frac{\mathscr{E}_p}{t_p}, \tag{17a}$$

which comes from Eqs. (9) and (10). For this special case, it is convenient to define the following dimensionless pulse parameters:

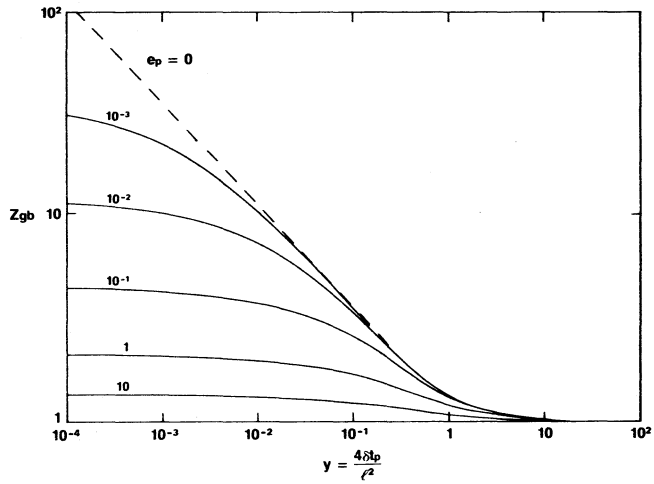

FIG. 10. Theoretical dependence of Z_{gb} on dimensionless pulse width for the ideal microstructure [Fig. 9(c)] and $\alpha \to \infty$ for several values of dimensionless pulse energy [Eq. (18b)]. The limiting ideal case of zero-electrical-resistivity grains is shown as the broken line. For finite resistivity and pulse energy, there are three distinct regimes (see text).

$$j_p = \frac{l}{\sigma v_0} J_p, \tag{18a}$$

$$e_p = \frac{4\delta}{\sigma v_0^2} \mathscr{E}_p, \tag{18b}$$

in addition to the dimensionless pulse width defined in Eq. (14). With these definitions

$$c = \frac{j_p^2 y}{e_p}, \tag{16b}$$

where j_p is determined by solving

$$j_p^2 + j_p \left(\frac{j_p}{j_0} \right)^{1/\alpha} = \frac{e_p}{y}. \tag{17b}$$

Equations (15)–(17) give the theoretical dependence of Z_{gb} on $\mathscr{E}_p$ and t_p for the ideal microstructure.

An analytically soluble special case which retains the essence of the phenomenon of interest is the $\alpha \to \infty$ limit of Eq. (17). In this limit, the solution of Eq. (17b) when substituted into Eq. (16b) gives

$$c = [(1+z)^{1/2} - z^{1/2}]^2, \tag{19}$$

where $z = y/4e_p$. Equations (19) and (15) are used to plot Z_{gb} as a function of y for several values of e_p in Fig. 10. The $c = 0$ (i.e., $e_p \to 0$) limit is also shown. It is apparent that as long as $e_p < 1$ there are three distinct regimes:

(i) the long-pulse-width regime in which $Z_{gb} = 1$, independent of y or e_p.

(ii) A short-pulse-width regime where

$$Z_{gb} \simeq 2\pi^{-1/2} y^{-1/2}, \tag{20}$$

independent of e_p. This is the regime where Z_{gb} follows the $e_p = 0$ curve.

(iii) A very-short-pulse-width regime ($y \to 0$) in which the limiting value of Z_{gb} is given by

$$Z_{gb} \simeq 1 + 2\pi^{-1/2} e_p^{-1/2}, \tag{21}$$

independent of y. The transition between regimes 1 and 2

occurs at $y \simeq 4/\pi$, while the transition between regimes 2 and 3 occurs at $y \simeq e_p$.

At first glance it may seem desirable from the standpoint of applications to reduce Z_{gb} for a given pulse width by increasing e_p (e.g., by contriving to decrease the grain conductivity [see Eq. (18b)]). However, this decrease is obtained by dissipating more energy in the grains, that is, by an increasing reversion to Ohmic behavior which defeats the clamping properties of the varistor. Thus, improvement in the performance of the ideal-microstructure varistor must be sought in reducing the susceptibility of the individual grain boundaries to thermal degradation, not by avoiding dissipating energy in them.

The experimentally measured values of Z_{gb} in Figs. 7 and 8 lie on a curve like the $e_p = 0$ curve in Fig. 10 so the energies and pulse widths were such that effectively all the energy dissipation was in the grain boundaries. Assuming a voltage drop of 2 V per boundary and the measured value of $F = 75$ V/mm at $J = 1$ mA/cm^2 for our experimental varistors, one finds $l = 27\,\mu$. Also, a good value for δ is $\delta = 0.103$ cm^2/sec. Thus the value of y at the point where the slope changes in Figs. 7 and 8 may be calculated from Eq. (14) as $y = 170$. This is more than two orders of magnitude greater than the value of $y = 4/\pi$ expected for the ideal microstructure modeled in this section. This discrepancy may be resolved by taking into account departures from the ideal microstructure.

B. Realistic microstructure

Thickness variations in the intergranular phase probably cause the characteristic electrical breakdown to occur only over a fraction of the total grain-boundary area as indicated schematically in Fig. 9(d). If Q is the average heat flux into the grain from all of the intergranular phase, then the actual heat flux at the *active* grain boundary is Q/γ where γ is a microstructural parameter defined by

$$\gamma = \frac{\text{active grain-boundary area}}{\text{total grain-boundary area}}. \tag{22}$$

This parameter obeys $\gamma \leqslant 1$, with $\gamma = 1$ only for the ideal microstructure studied above.

We next consider how Z_{gb} will be changed in each of the three regimes identified above with this modification to the model:

(i) In the long-pulse-width regime there will be sufficient time for the heat to diffuse throughout the microstructure during a pulse, just as in the ideal microstructure, so $Z_{gb} = 1$.

(ii) In the ideal model's $t_p^{-1/2}$ (short-pulse-width) regime, dissipation in the grains is negligible (effectively $\sigma \to \infty$) so we may use Eqs. (9), (14), and (20) to write

$$\Delta T_{gb} = 2\pi^{-1/2} y^{-1/2} \Delta T_{ave} = 2Q\left(\frac{t_p}{\pi K \rho C}\right)^{1/2}. \tag{23}$$

The fact that Eq. (23) is independent of l shows that in this regime a grain boundary is uninfluenced by its neighboring boundaries. Equation (23) is the solution for a single boundary embedded in an infinite grain. For short pulses, active boundary segments in the realistic model will also be uninfluenced by each other and ΔT_{gb} will have exactly the same form as Eq. (23) except that Q will be replaced by Q/γ. Thus, the form for Z_{gb} in the short-pulse-width regime of the realistic microstructure will be

$$Z_{gb} \simeq 2\pi^{-1/2}\gamma^{-1} y^{-1/2}. \tag{24}$$

(iii) In the very-short-pulse-width regime the partition of the dissipated energy between the grains and the grain boundaries must be considered, that is, the factor c in Eqs. (15) and (16) must be evaluated for the realistic microstructure. Levinson and Philipp[3] show that the grain resistivity measured by a high-current pulse technique is higher than that measured by high-frequency or infrared-reflection techniques because of the spreading resistance at the points of contact between the ZnO grains. That is, if the voltage drop across a grain is lJ_p/σ in the ideal microstructure, it is $l^2 J_p/\sigma d$ in the realistic microstructure, where d is the diameter of the contact area (the active part of the grain boundary). We assume one "inlet" and one "outlet" contact of diameter d per grain, so $\gamma = \pi d^2/4l^2$. When this is taken into account, Eq. (17b) becomes

$$\frac{1}{2}\left(\frac{\pi}{\gamma}\right)^{1/2} j_p^2 + j_p\left(\frac{j_p}{\gamma j_0}\right)^{1/\alpha} = \frac{e_p}{y} \tag{25}$$

and

$$c = \frac{1}{2}\left(\frac{\pi}{\gamma}\right)^{1/2} \frac{j_p^2 y}{e_p}. \tag{26}$$

When Z_{gb} is evaluated in the $\alpha \to \infty$ and $y \to 0$ limiting case via Eqs. (24) and (15), we find

$$Z_{gb} = 1 + 2^{3/2}\pi^{-3/4}\gamma^{-3/4} e_p^{-1/2}. \tag{27}$$

In general, the coefficient of $\gamma^{-3/4} e_p^{-1/2}$ will depend somewhat on the number and size of the contacts per grain but will be near unity. From Eqs. (24) and (27), the transition between regimes (i) and (ii) occurs at $y = 4/\pi\gamma^2$, while the transition between regimes (ii) and (iii) occurs at $y = \frac{1}{2} e_p (\pi/\gamma)^{1/2}$.

Since $\gamma \leqslant 1$, the effect of the nonideal microstructure is to shift the portion of the curves in Fig. 10 with slope $-\frac{1}{2}$ to the right [Eq. (24)] and to raise the level of the horizontal asymptotes for the very-short-pulse-width regime [Eq. (27)]. Thus the very-short-pulse-width regime is less likely to be observed in a realistic microstructure, while the short-pulse-width regime will occur for longer pulse widths, as compared to the ideal microstructure. For our varistors, Figs. 7 and 8 show that all of the data lie in the short- and long-pulse-width regimes, and the value of y (= 170) at the break in the slope of the experimental curves leads to a value of $\gamma = 8.7\%$.

The simple picture of Fig. 9(d) would indicate that in the neighborhood of 9% of the grain-boundary area is electrically active, in good agreement with the results of the high-current measurements of Levinson and Philipp.[3] Since the $t_p^{-1/2}$ law depends on the local thermal transport properties near an isolated active grain-boundary segment, a similar result would also obtain for randomly oriented active grain boundaries distributed randomly throughout the ceramic body, but the interpretation of γ may change accord-

ing to the distribution. Nonetheless, γ remains an index of the quality of the microstructure, with $\gamma = 1$ representing the ideal.

IV. SUMMARY AND CONCLUSIONS

There are two factors which bear on pulse-degradation performance:

(a) The electronic structure of the active grain-boundary segments. This determines the amount of degradation caused by a given temperature rise at the active grain-boundary segments during a pulse.

(b) The influence of the microstructure on the thermal transport properties of the composite. The thermal transport properties determine the actual temperature rise at active grain-boundary segments as a function of two independent pulse parameters. This effect is embodied in Z_{gb}, the grain-boundary temperature-magnification factor, which is the focus of this paper.

The electronic structure of the active grain boundaries is dramatically changed in a low-temperature (600 °C) oxygen anneal which improves the resistance to pulse degradation. This anneal leaves the microstructure unchanged.

The microstructurally dependent parameter Z_{gb} has three regimes: (i) long pulse widths, (ii) short pulse widths, and (iii) very short pulse widths, each with its own characteristic pulse width and pulse energy dependence. It is necessary to introduce a single parameter which accounts for the nonideality of the microstructure to explain our data in terms of the model.

ACKNOWLEDGMENT

We wish to thank Val Krehbiel for his careful work in obtaining the pulse-degradation data.

[1]L.M. Levinson and H.R. Philipp, J. Appl. Phys. **46**, 1332 (1975).
[2]L.M. Levinson and H.R. Philipp, J. Appl. Phys. **47**, 1117 (1976).
[3]L.M. Levinson and H.R. Philipp, J. Appl. Phys. **47**, 3116 (1976).
[4]H.R. Philipp and L.M. Levinson, J. Appl. Phys. **48**, 1621 (1977).
[5]J.D. Levine, CRC Crit. Rev. Solid State Sci. **5**, 597 (1975).
[6]J. Bernasconi, H.P. Klein, B. Knecht, and S. Strässler, J. Electron. Mater. **5**, 473 (1976).
[7]P.R. Emtage, J. Appl. Phys. **48**, 4372 (1977).
[8]P.L. Hower and T.K. Gupta, J. Appl. Phys. (to be published).
[9]H.R. Philipp and L.M. Levinson, J. Appl. Phys. **47**, 1112 (1976).
[10]J. Crank, *The Mathematics of Diffusion* (Oxford U.P., New York, 1956), p. 58.